Nonequilibrium Dynamics of Long-Range Interacting Fermions

Nonequilibrium Dynamics of Long-Range Interacting Fermions

T. Zwettler,[1] G. Del Pace,[1] F. Marijanovic,[2] S. Chattopadhyay,[2,3] T. Bühler,[1] C.-M. Halati,[4] L. Skolc,[2] L. Tolle,[5,4] V. Helson,[1] G. Bolognini,[1] A. Fabre,[1] S. Uchino,[6] T. Giamarchi,[4] E. Demler,[2] and J. P. Brantut[1]

[1]*Institute of Physics and Center for Quantum Science and Engineering, Ecole Polytechnique Fédérale de Lausanne (EPFL), CH-1015 Lausanne, Switzerland*
[2]*Institute for Theoretical Physics, ETH Zürich, CH-8093 Zürich, Switzerland*
[3]*Lyman Laboratory, Department of Physics, Harvard University, Cambridge, Massachusetts 02138, USA*
[4]*Department of Quantum Matter Physics, University of Geneva, Quai Ernest-Ansermet 24, 1211 Geneva, Switzerland*
[5]*Physikalisches Institut, University of Bonn, Nussallee 12, 53115 Bonn, Germany*
[6]*Faculty of Science and Engineering, Waseda University, Tokyo 169-8555, Japan*

(Received 16 December 2024; accepted 9 April 2025; published 10 June 2025)

A fundamental problem of out-of-equilibrium physics is the speed at which the order parameter grows upon crossing a phase transition. Here, we investigate the ordering dynamics in a Fermi gas undergoing a density-wave phase transition induced by quenching infinite-range, cavity-mediated interactions. We observe, in real time, the exponential rise of the order parameter and track its growth over several orders of magnitude. Remarkably, the growth rate can exceed the Fermi energy by an order of magnitude, consistent with predictions from a linearized instability analysis. This case contrasts with the ordering process driven by short-range interactions. We then generalize our results to linear interaction ramps, where deviations from the adiabatic behavior are captured by a simple dynamical ansatz. Our study offers a paradigmatic example of the interplay between strong short- and long-range interactions in quantum nonequilibrium dynamics.

DOI: 10.1103/PhysRevX.15.021089 Subject Areas: Atomic and Molecular Physics

I. INTRODUCTION

Understanding the coherent evolution of many-body systems crossing a phase transition is an ubiquitous problem in physics, arising in a wide range of contexts, including inflation [1], photoinduced states in solid-state physics [2,3], and adiabatic quantum computing [4]. A central question is the timescale over which the order of a symmetry-broken state emerges, bridging the gap from microscopic instabilities to macroscopic ordering.

Quench experiments, in which an external control parameter is abruptly changed, are among the most powerful tools for probing nonequilibrium dynamics. They are particularly suited for studying phase transitions in quantum gases, where the quench duration can be shorter than intrinsic timescales of the system. In short-range interacting atomic systems, two main features have been observed: (i) After quenching across a phase transition, the time evolution of long-range order is dominated by the formation and relaxation of defects [5–12]. These processes depend on the general properties of the transition but not on the microscopic instabilities that trigger it. (ii) The dynamics of short-range or short-time correlations occur at the scale of the Fermi time for a broad range of phenomena, from the formation of short-range pairs close to Feshbach resonances [13,14] to losses [15–18] or magnetic correlations [19,20]. On general grounds [21], any dynamics driven by contact interactions saturates at the scale of the Fermi time, which is the fastest microscopic timescale in a Fermi gas. Lastly, upon continuously ramping through a phase transition at finite speed, the dynamics of order formation follows the Kibble-Zurek scenario [22], where the defect dynamics is dictated by a power-law behavior of the underlying relevant timescales and length scales.

The recent advent of fermionic systems with controlled long-range interactions [23–26] opens the possibility to study far-from-equilibrium dynamics of order parameters in a nonlocal setting [27–29]. There, both the paradigms of defect formation and the upper limit set by the Fermi time to relaxation rates are challenged [30]. In fact, long-range interactions disfavor defect formation, which is completely suppressed in the regime of infinite-range interaction. This finding raises the prospect of observing the development of a microscopic instability without it being obscured by the

defect dynamics. An intriguing situation can then be anticipated for the timescales of the dynamics: Atomic ordering requires atomic motion, which is constrained by the Pauli exclusion principle or Cooper pairing; however, interactions with a range exceeding the interparticle spacing are not affected by quantum statistics, so the Fermi time may not play the same role.

Here, we exploit the unique settings of cavity quantum electrodynamics to record quantum trajectories of a strongly interacting Fermi gas within an optical cavity undergoing density-wave (DW) ordering after a quench of long-range atom-atom interactions. In this system, virtual cavity photons mediate infinite-range interactions while rare, spontaneous photon leakage events carry real-time information about the order parameter dynamics [31–35]. Upon quenching the system above the critical point, we directly observe the exponential growth of order over two decades, tracking it over a wide range of control parameters. The critical point is determined by the interplay between Pauli exclusion and contact interactions [26]. However, we observe a growth rate exceeding the Fermi energy by up to an order of magnitude. This finding suggests that Fermi statistics no longer influences the dynamics, in sharp contrast with quenched short-range interactions. The experiments are well described by a linear instability analysis, which allows us to identify the role of high-energy modes that are negligible around the critical point but dominate the growth rate for deep quenches. It also suggests that the fastest growth rates are determined by sum rules rather than Fermi energy. Finally, we examine the response to a linear ramp of long-range interaction strength and find that the ordering threshold shifts with the ramp speed following a power law. We show that this behavior is well explained by a simple adiabatic dynamical ansatz based on the separation of photonic and atomic timescales. This ansatz links the behavior to the growth rate dependence on interaction strength and differs strongly from predictions based on Kibble-Zurek scaling. All our findings are robust against variations of contact interactions across the Feshbach resonance, suggesting that the results are a generic feature of the nonequilibrium evolution of long-range interacting systems.

II. EXPERIMENTAL SYSTEM

We produce strong long-range interactions in a unitary Fermi gas by placing the atoms in a high-finesse Fabry-Perot cavity in the presence of side pumping. We start the experiments with a spin-balanced, degenerate Fermi gas of ^{6}Li close to a Feshbach resonance, trapped within the fundamental mode of a high-finesse optical cavity (see Ref. [36] and Appendix A for details). The gas has a Fermi energy of $E_F = h \times 20.7$ kHz. We illuminate the cloud from the side with a linearly cross-polarized, retroreflected pump beam as illustrated in Fig. 1(a). The pump beam is detuned by $-2\pi \times 47.690$ GHz from the atomic D_2 transition but has a close detuning of $\tilde{\Delta}_c \sim$ MHz from a dispersively shifted cavity resonance, such that direct Rayleigh scattering in the cavity is off resonant but second-order photon-exchange processes dominate, yielding an atom-atom interaction extending over the entire mode volume of the cavity. Photon exchanges impart

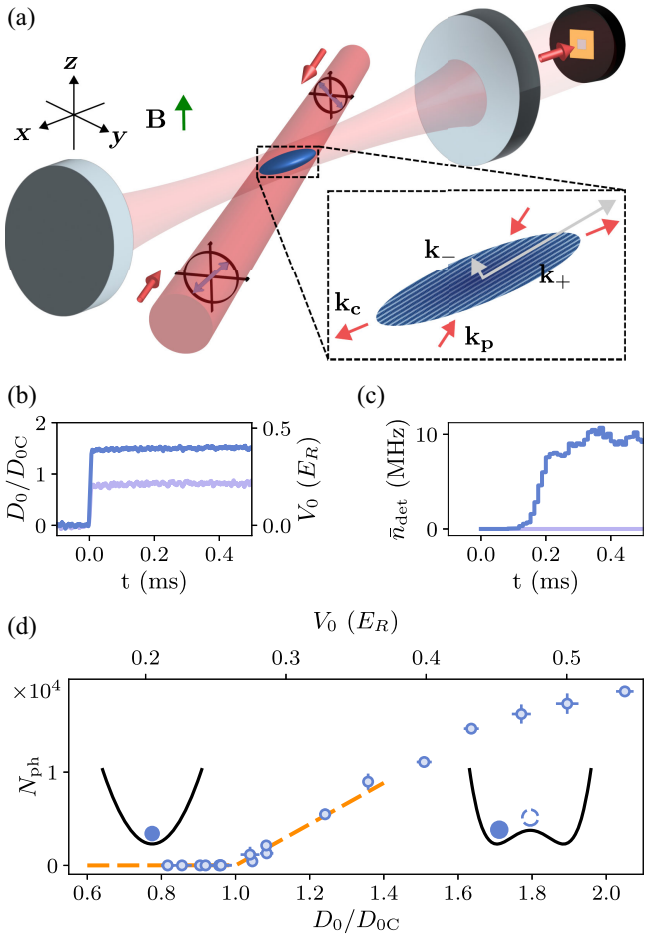

FIG. 1. Concept of the experiment. (a) Strongly interacting Fermi gas of ^{6}Li, residing inside a high-finesse optical resonator, illuminated by a retroreflected pump laser with cross-polarization. Pump photons dispersively couple to atomic motion and impart momentum kicks of magnitude $k_\pm = |\mathbf{k}_p \pm \mathbf{k}_c|$ on atoms through scattering from the pump into the cavity and vice versa. (b) Long-range interaction strength D_0 quenched across the critical point D_{0C} by suddenly switching on the pump beam with a strength V_0 in units of the recoil energy E_R, here shown for $D_0/D_{0C} = 1.51(2)$ (——) and $D_0/D_{0C} = 0.82(2)$ (——). (c) Photon flux exiting the cavity measured on a single photon counter following the quench displayed in panel (b). (d) Cumulative count of photons N_{ph} (○) detected during a fixed time window of 2 ms subsequent to the starting point of the quench. We identify D_{0C} by the onset of a finite N_{ph} and extract its value by a fit of the kink (- - -). The critical value coincides with the onset of an instability of the symmetric equilibrium in the free energy of the system [26]. The error bar represent 1 standard deviation.

discrete momentum kicks of $k_\pm = |\mathbf{k}_p \pm \mathbf{k}_c|$ to the atoms, where $\mathbf{k}_{p,c}$ are the wave vectors of the pump and cavity photons, respectively [see Fig. 1(a)]. The angle of 18° between the pump and cavity axis results in the hierarchy $k_- \ll k_F \ll k_+$, with the Fermi wave vector $k_F = \sqrt{2mE_F}/\hbar$. The resulting long-range interaction potential between atoms reads (see Appendix C):

$$\hat{D}(\mathbf{r},\mathbf{r}') = D_0[\cos(\mathbf{k}_+ \cdot (\mathbf{r}-\mathbf{r}')) + \cos(\mathbf{k}_- \cdot (\mathbf{r}-\mathbf{r}')) + \cos(\mathbf{k}_+ \cdot \mathbf{r} + \mathbf{k}_- \cdot \mathbf{r}') + \cos(\mathbf{k}_- \cdot \mathbf{r} + \mathbf{k}_+ \cdot \mathbf{r}')], \quad (1)$$

with $D_0 \propto V_0/\tilde{\Delta}_c$, and V_0 is the light shift induced by the pump beam. In contrast with Refs. [25,37], we operate in the strong dispersive coupling regime where the photon decay rate κ is much smaller than both the dispersive shift and $\tilde{\Delta}_c$, such that dissipation due to cavity-photon losses does not dominate the phase diagram nor the dynamics [38]. Above a critical long-range interaction strength, the system undergoes a quantum phase transition into a DW-ordered phase [25,26] at wave vectors $\mathbf{k}_\pm$ determined by the cavity and pump geometry. If the interaction strength is increased above the critical value, the system finds itself in an unstable equilibrium and density-wave order appears, as shown in Fig. 1(d). The single-mode nature of the cavity enforces ordering at all spatial locations simultaneously. This instability arises from an inversion of the curvature in the free-energy landscape, suggesting an analogy with a simple inverted harmonic oscillator, which is a model ubiquitous across different fields of physics [39].

III. QUENCH DYNAMICS

We perform a sudden quench of D_0 in the atom-cavity system by switching on the pump beam power from zero to a finite value at time $t = 0$ at fixed $\tilde{\Delta}_c$, as presented in Fig. 1(b), and we record the photon flux $\bar{n}_{det}$ leaking from the cavity over a single realization using a single photon counter (SPC). The cross-polarization used for the pump beam ensures that there is no optical lattice along the pump direction. Consequently, no atomic dynamics is initiated along the direction $\mathbf{k}_p$. For $D_0 > D_{0C}$, we observe that $\bar{n}_{det}$ builds up in time, as shown in the examples in Fig. 1(c). In our regime of $E_F \ll \hbar\tilde{\Delta}_c$, the cavity field follows the DW order adiabatically, such that photon traces represent individual quantum trajectories of the ordering process in the cloud [35]. Integrating $\bar{n}_{det}$ over time after a quench allows us to precisely determine the phase boundary D_{0C}, as presented in Fig. 1(d).

To understand the dynamics of ordering, we systematically record individual time traces of $\bar{n}_{det}$ following a D_0 quench. After applying a moving-average filter, we analyze each time trace. Typical curves and their exponential fit are presented in Fig. 2, for quenches of D_0 between D_{0C} and $15 \times D_{0C}$. We observe an uninterrupted exponential growth

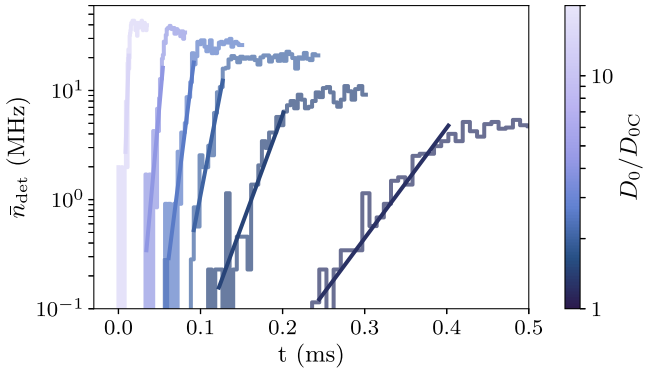

FIG. 2. Exponential growth of the instability. Photon flux $\bar{n}_{det}$ for different single experimental realizations, following a sudden long-range interaction quench to values of D_0 ranging from D_{0C} to $15 \times D_{0C}$. The individual traces exhibit exponential growth across all parameters, spanning more than an order of magnitude in photon flux before saturation occurs. Each photon flux trace is represented as a binwise step function, fitted with an exponential curve (solid lines) to extract the growth rate.

over more than 1 order of magnitude in the photon flux. This observation is the generic behavior of ordering at early times in the unstable regime [5], which we observe here with a high dynamic range thanks to the cavity-QED setting. We find that the growth of order is well described by an exponential for all parameters explored. Remarkably, the exponential growth persists over more than a decade in $\bar{n}_{det}$, with no indication of a change in behavior until saturation is reached. The long-range character of the interactions prevents the proliferation of defects in the ordering process, such that the runaway evolution of the unstable oscillator can proceed without yielding any defect coarsening dynamics. As a result, the ordering is described by a single growth rate α. We find that this behavior is not restricted to our bulk, three-dimensional Fermi gas; it is also observed in numerical simulations for one-dimensional systems coupled to a classical cavity mode (see Appendix E).

We now proceed to systematically explore the evolution of α in a unitary Fermi gas quenched into the DW-ordered phase, for D_0 up to $30 \times D_{0C}$. The growth rate is obtained by a fit of individual photon flux traces. The results are presented in Fig. 3(a) for three different choices of $\tilde{\Delta}_c$. As expected, curves for these three detunings collapse, showing that the only relevant parameter is the long-range interaction strength. For D_0 approaching D_{0C}, α tends to zero, which is a manifestation of the critical slowing down close to the phase transition [30]. Deeper in the DW-ordered phase, α monotonically increases with D_0 over 2 orders of magnitude, showing no sign of saturation. It reaches and eventually exceeds the Fermi energy by about an order of magnitude for the largest D_0, meaning that the system orders much faster than the local fermionic timescale. Effectively, the long-range character of the

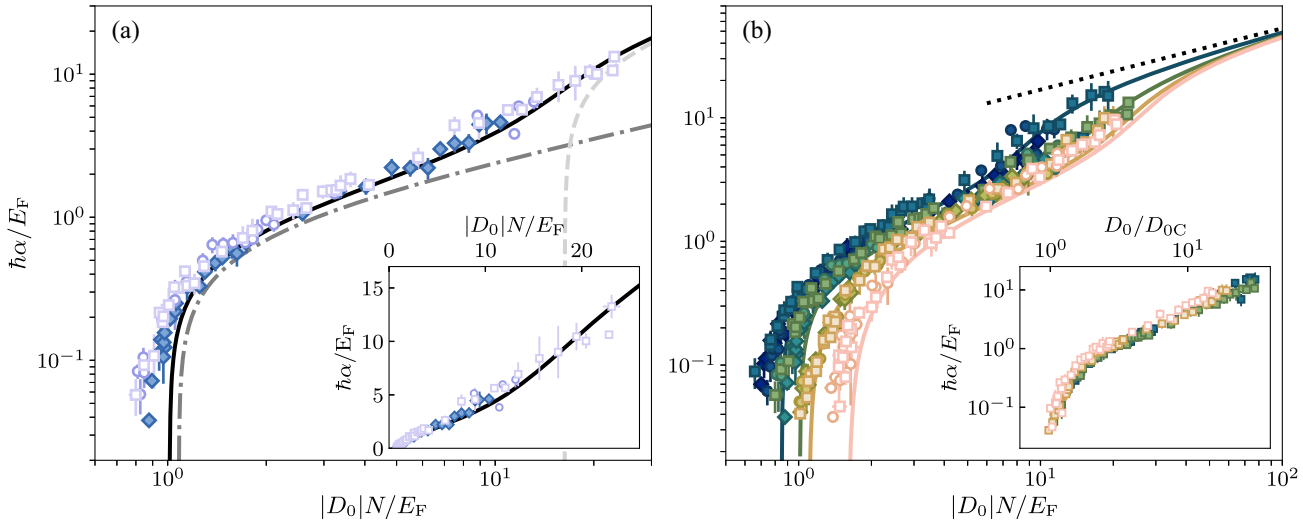

FIG. 3. Instability growth rates. (a) Instability growth rate α in units of the Fermi energy E_F at unitarity as a function of D_0 for different pump-cavity detunings $\tilde{\Delta}_c$: −1.4 MHz (□), −2.5 MHz (○), and −3.4 MHz (◇). Theoretical prediction based on an instability analysis including trap averaging (——), with the individual contributions of k_+ (- - -) and k_- (—·—). (b) Growth rates away from unitarity at $\tilde{\Delta}_c$: −3.4 MHz (◇), −2.5 MHz (○), −1.4 MHz (□), $1/k_F a$: 1.1 (◇○□), 0 (◇○□), and −0.7 (◇○□) and for a noninteracting Fermi gas at $\tilde{\Delta}_c = -1.3$ MHz (○) and −0.8 MHz (□). Solid lines show the corresponding theoretical predictions. Note that α converges to a limiting value given by the f-sum rule (·····) for $D_0 \longrightarrow \infty$. The inset shows the same data with D_0 normalized by the value D_{0C}, observed for the corresponding interaction strength and cavity detuning. The error bars represent 1 standard deviation.

interactions circumvents the effects of the Pauli exclusion on interactions.

To uncover the microscopic origin of this behavior, we model the early-time evolution following the quench using a linear-response theory (see Appendix D). This framework amounts to a linear instability analysis, which naturally yields an exponential growth of the order parameter for the unstable polaritonic mode. The growth is seeded by either initial fermionic density fluctuations or cavity shot noise and coherently amplified by the unitary dynamics. This approach leads to the following implicit equation for α:

$$1 = \frac{D_0 N}{8} \sum_{q=\pm k_\pm} \int_{-\infty}^{\infty} \frac{d\omega}{\pi} \frac{\omega \, \mathrm{Im}[\chi^R(q,\omega)]}{\alpha^2 + \omega^2}, \qquad (2)$$

with $\chi^R(q,\omega)$ the retarded density-density response function at momentum q and frequency ω, evaluated prior to the quench for the equilibrium gas at unitarity and including averaging over the harmonic trap. The above expression is valid in the limit of $\alpha/\Delta_c \ll 1$, which is relevant for the experimental parameter regime. For higher-order corrections and details, see Appendix D. The k_- mode has the lowest energy, and it controls the location of the phase transition. It corresponds to sound waves or pair-breaking excitations on the Fermi surface, and its natural scale is the Fermi energy, the maximum width of the pair-breaking continuum. This fact motivates the normalization of the data by E_F in Fig. 3. In contrast, the k_+ mode only contributes at high frequencies, away from criticality, and is weakly affected by Pauli exclusion and atom-atom interactions.

Using the random-phase-approximation result for $\chi^R(k_\pm,\omega)$ at unitarity [40], we obtain a prediction for the growth rate for all values of D_0 without free parameters, as plotted in Fig. 3(a) as a solid black line. The agreement of theory with experimental data is very good over the whole range of parameters. This analysis also highlights the role of the k_- and k_+ modes in the dynamics, and their individual contribution is presented as dashed and dotted-dashed lines in Fig. 3(a). Since $k_+ \gg k_-$, we observe a crossover between the k_--dominated dynamics close to the critical point and the k_+-dominated dynamics at very large D_0.

We now generalize these investigations to Fermi gases away from unitarity through the crossover between the Bose-Einstein condensate (BEC) and Bardeen-Cooper-Schrieffer (BCS) superfluids for finite positive and negative scattering length a, as well as for an ideal, fully polarized Fermi gas. The results are presented in Fig. 3(b). The critical point changes with interaction strength, and so does the growth rate. In all cases, the theory is in quantitative agreement with the experimental data. After normalizing the long-range interaction strength of each curve by D_{0C}, we observe a collapse of the curves within our signal-to-noise ratio [inset of Fig. 3(b)] across the two decades of growth rate explored by the system. This behavior also extends to the noninteracting Fermi gas. This striking similarity suggests that, while the microscopic details of the gas are important to determine D_{0C}, the dynamics of ordering is mostly governed by the long-range interactions.

Our theoretical model suggests a possible set of explanations for the independence of growth rates on contact

interactions. For $\alpha \to \infty$, Eq. (2) simplifies to the f-sum rule, which enforces a universal, interaction, and quantum-statistics independent growth rate. The corresponding value is presented in Fig. 3(a) as a dotted line, and Fig. 3(b) shows it in the asymptotic regime, which is not reached in our experiments. For lower growth rates, deviations from the f-sum rule appear due to the weak dependence of $\chi^R(k_+, \omega)$ on interactions. For D_0 closest to D_{0C}, the growth rate is controlled by the critical behavior of the system, primarily determined by the zero-frequency response function at k_-, which approaches the compressibility for $k_- \ll k_F$ [26]. In our case, the averaging over the harmonic trap smoothens out the moderate quantitative differences to a range comparable with the experimental noise.

IV. RAMP DYNAMICS

We now utilize a ramp protocol in which the transition is crossed at a finite speed, as commonly used to investigate the dynamics of phase transitions [8]. After a similar preparation as in the quench protocol, we perform linear ramps of D_0 at finite speed $\dot{\epsilon}$ with $\epsilon = [(D_0 - D_{0C})/D_{0C}]$, as shown in Fig. 4(a). Throughout the linear ramp, time directly maps onto D_0, which allows us to identify for each $\dot{\epsilon}$ an apparent ordering threshold $D_{0,\mathrm{thr}}$, as presented in Fig. 4(b) (see Appendix B for details). We use the photon traces to extract the relative differences of the apparent threshold to the critical value $\epsilon_{\mathrm{thr}} = [(D_{0,\mathrm{thr}} - D_{0C})/D_{0C}]$ over four decades in speed. The results are presented in Fig. 4(c). As the speed increases, we observe a growing difference in the apparent ordering threshold, which occurs because the system orders at later relative times during the ramp at higher speeds. The smooth variations, spanning up to a tenfold increase in the threshold, are identical from noninteracting to strongly interacting fermions across the BEC-to-BCS crossover. At the lowest speeds, we observe a large noise in ϵ_{thr} and systematic deviations caused by atom losses during the ramp.

Here, ϵ_{thr} exhibits a consistent power-law behavior over more than 1 order of magnitude in speed. We substantiate this by fitting a power law to the different curves at unitarity, finite a, and for an ideal gas, as presented in Fig. 4(d). Such a power-law behavior could suggest an explanation in terms of a generalized Kibble-Zurek scenario [30,32,41], in which the instantaneous growth rate of the order parameter is integrated throughout the ramp protocol [42]. We fit the power-law behavior with $\epsilon_{\mathrm{thr}} \propto \dot{\epsilon}^{1/(1+\gamma)}$, as presented in Fig. 4(d). In the Kibble-Zurek framework, γ corresponds to the dynamical critical exponent, which characterizes the phase transition. We find an exponent of 0.73(14), strongly deviating from the value of 0.18 measured in Ref. [32] for the open Dicke model with rising pump ramps but in agreement with the value of 0.75 found there for decreasing ramps. It also differs from predicted mean-field values for closed ($\gamma = 0.5$) and open quantum systems ($\gamma = 1$) [30,43–45].

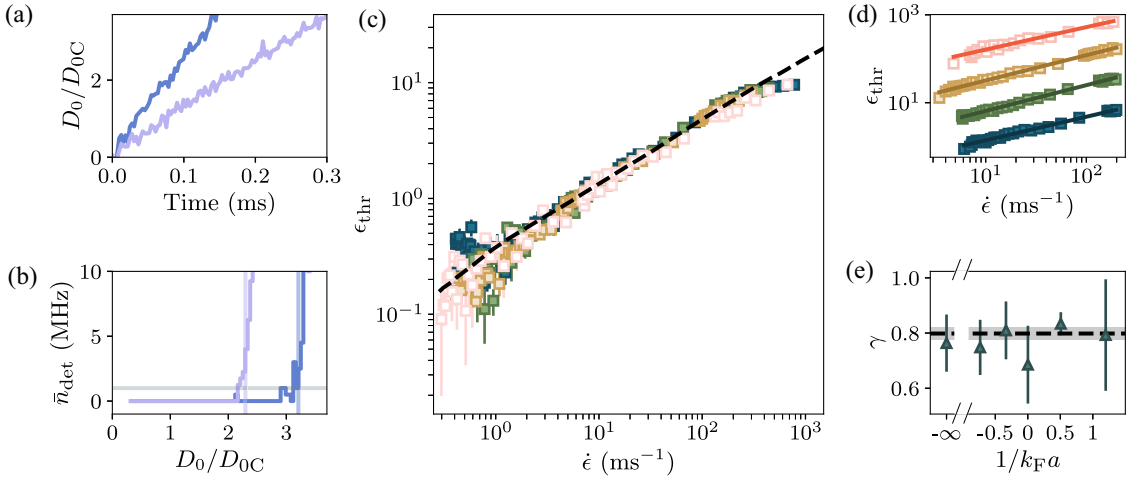

FIG. 4. Linear ramps of long-range interactions. (a) Linear ramps of D_0 with different speeds of $\dot{\epsilon} = 10.7$ ms^{-1} (——) and 21.7 ms^{-1} (——). Each line represents the pump-power ramp as experimentally measured. (b) Cavity photon leakage $\bar{n}_{\mathrm{det}}$ during the ramp, from which we extract the long-range interaction strength $D_{0,\mathrm{thr}}$ (vertical lines) to reach a threshold count rate of 1 MHz (——). (c) Relative difference ϵ_{thr} of threshold to the critical point as a function of the quench rate $\dot{\epsilon}$ for $\tilde{\Delta}_c = -1.4$ MHz at $1/k_F a$: 1.1 (□), 0 (□), and −0.7 (□) and for the polarized Fermi gas (□). Here, (- - -) shows the behavior as a function of the ramp speed predicted from the dynamical ansatz, based on the data of Fig. 3 (see text for details). (d) Power-law fits to ϵ_{thr} for the different interaction strengths reported in panel (c), offset by a multiplicative factor of 5 for clarity. (e) Power-law exponents for different short-range interaction strengths $1/k_F a$ (△), where the point at $-\infty$ represents the polarized, noninteracting Fermi gas. Each data point corresponds to the weighted average, and the error bar shows the standard deviation among the exponents γ obtained over datasets at different $\tilde{\Delta}_c$. We also indicate the critical exponent determined from fitting the dynamical ansatz (- - -), together with its fit error reported as the shaded region. Unless otherwise stated, error bars on data points for each panel represent 1 standard deviation.

Rather than connecting the ramp response to the critical behavior as in the Kibble-Zurek scenario, we can explain the observed power-law based on the knowledge of the growth rate after a quench. Knowing the exponential scaling law of Fig. 3 for a given D_0 offers the possibility to compare the ramp speed with the instantaneous growth rate at each point in time, thus quantifying the deviations from the adiabatic behavior. This process leads to a first-order differential equation ansatz for the photon flux leaking from the cavity as a function of time in the presence of time-varying D_0:

$$\frac{\mathrm{d}\bar{n}_{\mathrm{det}}}{\mathrm{d}t} = \alpha(t)\bar{n}_{\mathrm{det}}(t). \tag{3}$$

Here, we propose the adiabatic dependence $\alpha(t) = \alpha[D_0(t)]$, which generalizes the exponential law while keeping the dynamics independent of any microscopic detail beyond the determination of α. Direct integration of Eq. (3) using the data of Fig. 3(b) yields a prediction for the photon flux throughout the ramps, as presented as a dashed line in Fig. 4(c). We have combined all the data of Fig. 3(b), as they show no significant difference within our signal-to-noise ratio. The agreement is excellent across most of the parameter range, except at the highest speeds, further demonstrating the universal character of the dynamical properties. Together with our previous analysis of the growth rate, this agreement suggests that ramp responses are ultimately determined by the response function of the equilibrium Fermi gas in the initial state.

Interestingly, our results support the extended interpretation of the Kibble-Zurek picture [42]: It ties the scaling of the ramp response to the growth rate of the order parameter and thus to the equilibrium properties of the gas without long-range interactions, following our theoretical interpretation. A manifestation of this feature is the role of the high-energy mode at k_+ as observed in Fig. 3, which contributes to our dynamical ansatz throughout integration but is negligible for the determination of the critical point.

V. CONCLUSION AND PERSPECTIVES

In conclusion, our thorough investigation of the ordering dynamics of long-range interacting fermions suggests a distinct classification for these systems compared to their short-range interacting counterparts. Here, the entire ordering process follows an exponential growth mechanism, weakly dependent on microscopic details. In short-ranged systems, the ramp protocol reflects the critical properties of the transition, as given by Kibble-Zurek prescriptions. However, in our setting, the long-ranged photon-mediated interactions enforce an infinite correlation length for the order parameter throughout the transition, nullifying the association between diverging spatial and temporal scales at criticality.

Beyond our theoretical analysis of the three-dimensional system, these general conclusions are also supported by our numerical simulations of simplified models in one and two dimensions (see Appendix E). Interestingly, we did not observe photon-number ringing in the early-time dynamics nor a late-time steady-state regime with high temperature throughout the parameter space explored in our experiments, in contrast with Ref. [37]. There, the sudden quench protocol was investigated in a regime of weak collective coupling and $\tilde{\Delta}_c \sim \kappa$. While our general framework cannot capture the late-time dynamics, we attribute the absence of ringing in our case to our operation in the regime $\tilde{\Delta}_c \gg \kappa > E_{\mathrm{F}}$. Beyond the context of cavity QED, our results also provide a framework for the description of Fermi gases interacting at finite range due to dipolar interactions or Rydberg dressing, where the interplay between the finite interaction range and the system size would give rise to a richer scenario.

By virtue of the ability of our cavity-QED system to record not only average time evolution but also single quantum trajectories, we have access to information in the noise and correlations of such signals. There, we anticipate that quantum effects, such as measurement backaction from the cavity and quantum noise in the gas, could arise in the form of deviations from the mean-field description.

ACKNOWLEDGMENTS

We thank Simon Jäger for discussions. The EPFL group acknowledges funding from the Swiss State Secretariat for Education, Research and Innovation (Grants No. MB22.00063 and No. UeM019-5.1). A. F. acknowledges funding from the EPFL Center for Quantum Science and Engineering. The ETH group acknowledges funding from the Swiss National Science Foundation Project No. 200021_212899; the Swiss State Secretariat for Education, Research and Innovation (Contract No. UeM019-1), and National Center of Competence in Research "SPIN." E. D. acknowledges funding from ARO Grant No. W911NF-21-1-0184. S. C. is grateful for support from the NSF under Grant No. DGE-1845298 and for the hospitality of the Institute of Theoretical Physics at ETH, Zürich. S. U. acknowledges funding from by JST PRESTO (JPMJPR235) and JSPS KAKENHI (JP21K03436). T. G. and C.-M. H. acknowledge support from the Swiss National Science Foundation under Division II Grants No. 200020-188687 and No. 200020-219400, and would like to thank the Institut Henri Poincaré (UAR 839 CNRS-Sorbonne Université) and the LabEx CARMIN (ANR-10-LABX-59-01) for their support. C.-M. H. acknowledges support, in part, from Grant No. NSF PHY-1748958 to the Kavli Institute for Theoretical Physics (KITP). L. T. acknowledges support from the Deutsche Forschungsgemeinschaft (DFG, German Research Foundation) under Projects No. 277625399—TRR 185 (B4) and No. 277146847—CRC 1238 (C05), and under

Germany's Excellence Strategy—Cluster of Excellence Matter and Light for Quantum Computing (ML4Q) EXC 2004/1–390534769.

DATA AVAILABILITY

The data that support the findings of this article are openly available [46].

APPENDIX A: EXPERIMENTAL PROCEDURE

We produce a strongly interacting Fermi gas of ^{6}Li comprising 5.68×10^5 atoms in the two lowest hyperfine states in the vicinity of the broad magnetic Feshbach resonance at 832 G. We make use of the apparatus described in our previous work [47,48], with modifications in the last evaporation stages as presented in Ref. [36], leading to a deeply degenerate gas trapped in an elongated harmonic trap with transverse frequencies $\omega_{y,z} = 430$ Hz and a longitudinal frequency of $\omega_x = 28$ Hz along the cavity axis.

As mentioned in the main text, the pump beam is operated in the atomic dispersive coupling regime but very close to a TEM_{00} cavity mode. We monitor the power sent on the atoms during each shot on a photodiode. The pump potential depth is calibrated in atomic recoil units $E_\mathrm{R} = \hbar^2 \mathbf{k}_\mathrm{p}^2/2m = h \times 73.67$ kHz by first performing a Kapitza-Dirac diffraction experiment on a molecular BEC at 690 G using a standing-wave pump beam with π polarization, obtaining the pump lattice depth $V_{0,\mathrm{KD}}$ [49]. We subsequently cancel the pump lattice by introducing linear, orthogonal polarizations for the pump beam and its back reflection as shown in Fig. 1(a), which we verify through the absence of diffraction peaks in the Kapitza-Dirac experiment. The geometry and properties of the pump are otherwise the same as in Ref. [26]. The lattice-free pump potential depth is given by $V_0 = V_{0,\mathrm{KD}}/2$.

The long-range interaction strength $D_0 \propto V_0/\tilde{\Delta}_\mathrm{c}$ can be tuned by varying the pump detuning from the dispersively shifted cavity $\tilde{\Delta}_\mathrm{c}$ or the pump potential depth V_0. The pump-cavity detuning $\tilde{\Delta}_\mathrm{c} = \Delta_\mathrm{c} - \delta_\mathrm{c}$ is chosen to largely exceed the cavity dispersive shift of $\delta_\mathrm{c} = -2\pi \times 1.5$ MHz and the cavity linewidth of $\kappa = 2\pi \times 77$ kHz. For sudden quenches, we switch on V_0 from zero to a finite value on a characteristic timescale of 1 μs, which is faster than the dissipative photon dynamics on the timescale $1/\kappa \approx 2$ μs and any atomic motion in the uniform state at $\hbar/E_\mathrm{F} \approx 7.7$ μs but slower than the coherent photon dynamics at $2\pi/\tilde{\Delta}_\mathrm{c}$.

After a quench, the photon flux leaking from the cavity is detected using a single-photon counter with an efficiency of approximately 3% [50].

APPENDIX B: DATA ANALYSIS

1. Analysis of sudden quenches

We extract the system response to sudden quenches by performing an exponential fit on the histograms of photon counts in the early time for each experimental realization. We apply a moving average before fitting to mitigate photon shot noise. The fit function is given by

$$\bar{n}_\mathrm{det}(t) = \bar{n}_0 e^{\alpha t}, \tag{B1}$$

with a seed flux value $\bar{n}_0$ and a growth rate α. The fit range is up to either 60% of the maximal value or a maximal count rate of 20 MHz, depending on which value is reached first. At count rates larger than 20 MHz, the photon flux traces are significantly distorted due to dead-time effects of the single-photon counter. The fit is performed as a linear fit on a log scale, therefore equally weighting low and high count rates in the least-square minimization.

2. Analysis of dynamic ramps

We extract the apparent ordering threshold $D_{0,\mathrm{thr}}$, at which the photon rate $\bar{n}_\mathrm{det}$ reaches 1 MHz, by fitting the onset of the acquired photon flux traces with a linear function:

$$\bar{n}_\mathrm{det}(t) = \theta(t - t_0) B (t - t_0), \tag{B2}$$

where $\theta(t)$ is the Heaviside function, and t_0 and B are fit parameters. From this fit, we obtain the time t_thr at which the photon flux exceeds 1 MHz, which is subsequently converted to a long-range interaction strength $D_{0,\mathrm{thr}}$ using the linear ramp shape. Thus, we perform a linear fit to the pump power, which is monitored for each realization on a photodiode, and use it to extract its power at t_thr, which we then convert into D_0. The same linear fit on the photodiode signal also provides a measurement of the ramp speed $\dot{\epsilon}$.

To extract the scaling exponent γ, we perform a power-law fit of ϵ_thr over a limited range of ramp speed $\dot{\epsilon}$ [see Fig. 4(d) of the main text]. In particular, we constrain the fit region up to $\dot{\epsilon} = 200\ \mathrm{ms}^{-1}$, which is the largest ramp speed at $1/k_\mathrm{F}a = -0.7$. On the other hand, ϵ_thr can be artificially increased by atom losses happening before reaching the threshold in the low speed limit [which is strongest for the data at $1/k_\mathrm{F}a = 1.1$ in Fig. 4(c)] because of the long duration of the pump-power ramp. We exclude the loss-dominated region at low speed by performing a two-step fit: We first fit ϵ_thr over the full range of $\dot{\epsilon}$ and then exclude all the points up to the $\dot{\epsilon}$ value where the residual of the first fit is 25%. The power-law fit performed over such a restricted range of $\dot{\epsilon}$ provides the best value of γ, and its corresponding fit error is typically on the order of 5%.

The method we use to obtain the optimal value of γ is subject to two sources of systematic error. First, both ϵ_thr and $\dot{\epsilon}$ are calculated from the measured value of $D_{0\mathrm{C}}$, which we extract as described above. To account for the systematic on γ reflected by the error on $D_{0\mathrm{C}}$, we repeat the power-law fit on $\epsilon_\mathrm{thr}(\dot{\epsilon})$ several times, employing, for each fit, a different value of the critical long-range interaction

strength in the confidence range of the measured D_{0C}. Calculating the standard deviation over the values of γ obtained from the different fits, we estimate the systematic error on the power-law exponent due to the finite precision on measuring D_{0C} to be on the order of around 1% for all the datasets. Second, a source of systematic error on γ arises from our selection of the range of $\dot{\epsilon}$ over which the fit is conducted. We estimate this contribution by releasing the fit range constraints and computing the standard deviation over the different values of γ obtained in the extended range of $\dot{\epsilon}$. In particular, to estimate the systematic, we let the fit range vary up to 1000 ms^{-1}, corresponding to the absolute largest ramp speed and down to the value of $\dot{\epsilon}$ where the residual of the first fit is 10%.

We estimate the systematic error on γ due to the choice of the fit range to be of the order of about 7% for all the datasets. The final error on γ is then calculated as the quadratic sum of the different error contributions: the fitting error on the best fit and the two systematic errors. The value of $\gamma = 0.73(14)$ reported in the main text corresponds to the weighted average and standard deviation over the γ values obtained for the datasets at different $\tilde{\Delta}_c$ and short-range interaction strength.

APPENDIX C: EFFECTIVE HAMILTONIAN

In this section, we derive the effective Hamiltonian describing the transversely pumped atom-cavity system. The Fermi gas inside the optical resonator is transversely pumped by a pump laser with a geometry as shown in Fig. 1. The pump beam and its back reflection are both in a coherent state with equal amplitude λ_p. Their linear and orthogonal polarizations are described by the unit vectors $\mathbf{e}_1 = 1/\sqrt{2}(\mathbf{e}_z - \mathbf{e}_p)$ and $\mathbf{e}_2 = 1/\sqrt{2}(\mathbf{e}_z + \mathbf{e}_p)$, with the polarization vector in the pump-cavity plane $\mathbf{e}_p = \cos(\phi)\mathbf{e}_y + \sin(\phi)\mathbf{e}_x$ and the angle of the pump to the cavity axis $\phi = \pi/10$. The atoms couple to two degenerate, standing-wave modes of the cavity described by the annihilation operators $\hat{a}_{y/z}$ with respective polarizations along y and z. The combined pump-cavity field is given by

$$\begin{aligned}\phi(\mathbf{r}) = &\cos(\mathbf{k}_c \cdot \mathbf{r})(\hat{a}_y \mathbf{e}_y + \hat{a}_z \mathbf{e}_z) \\ &+ \lambda_p (e^{i\mathbf{k}_p \cdot \mathbf{r}} \mathbf{e}_1 + e^{-i\mathbf{k}_p \cdot \mathbf{r}} \mathbf{e}_2). \end{aligned} \tag{C1}$$

The absence of vector polarizability in our experimental regime leads to the usual dispersive light-matter coupling of atomic density of both hyperfine states $\hat{n}(\mathbf{r}) = \sum_{\sigma=\uparrow\downarrow} \hat{n}_\sigma(\mathbf{r})$ to an effective pump-cavity potential [35] given by

$$H_{\mathrm{int}} = \int d\mathbf{r} \hat{n}(\mathbf{r}) \hat{V}_{\mathrm{eff}}(\mathbf{r}), \tag{C2}$$

where

$$\begin{aligned}\hat{V}_{\mathrm{eff}} = &V_0 + U_0(\hat{a}_y^\dagger \hat{a}_y + \hat{a}_z^\dagger \hat{a}_z)\cos^2(\mathbf{k}_c \cdot \mathbf{r}) \\ &+ \eta_0[i\cos(\phi)\cos(\mathbf{k}_c \cdot \mathbf{r})\sin(\mathbf{k}_p \cdot \mathbf{r})(\hat{a}_y - \hat{a}_y^\dagger) \\ &+ \cos(\mathbf{k}_c \cdot \mathbf{r})\cos(\mathbf{k}_p \cdot \mathbf{r})(\hat{a}_z + \hat{a}_z^\dagger)], \end{aligned} \tag{C3}$$

with lattice-free pump potential of depth V_0, the intracavity lattice depth per photon U_0, and $\eta_0 = \sqrt{U_0 V_0}$. The full Hamiltonian can then be recast in the form

$$\begin{aligned}\hat{H} = &\hat{H}_{\mathrm{at}} - \tilde{\Delta}_c(\hat{a}_y^\dagger \hat{a}_y + \hat{a}_z^\dagger \hat{a}_z) \\ &+ \eta_0[\cos(\phi)\hat{\Theta}_y(\hat{a}_y - \hat{a}_y^\dagger) + \hat{\Theta}_z(\hat{a}_z + \hat{a}_z^\dagger)], \end{aligned} \tag{C4}$$

where $\tilde{\Delta}_c = \Delta_c - \delta_c = \Delta_c - U_0 \int d\mathbf{r} n(\mathbf{r})\cos^2(\mathbf{k}_c \cdot \mathbf{r})$ is the detuning of the pump from the dispersively shifted cavity resonance and $\hat{H}_{\mathrm{at}}$ is the Hamiltonian of an interacting, harmonically trapped two-component Fermi gas. The potential offset created by the pump has been dropped. Furthermore, we introduce the density-wave operators for polarizations y and z, describing the modulation of the atomic density at wave vectors $\mathbf{k}_\pm = \mathbf{k}_p \pm \mathbf{k}_c$:

$$\begin{aligned}\hat{\Theta}_y &= \int d\mathbf{r} \cos(\mathbf{k}_c \cdot \mathbf{r}) \sin(\mathbf{k}_p \cdot \mathbf{r}) \hat{n}(\mathbf{r}) \\ &= \frac{1}{4}(\hat{n}_{\mathbf{k}_-} - \hat{n}_{-\mathbf{k}_-} - \hat{n}_{\mathbf{k}_+} + \hat{n}_{-\mathbf{k}_+}), \\ \hat{\Theta}_z &= \int d\mathbf{r} \cos(\mathbf{k}_c \cdot \mathbf{r}) \cos(\mathbf{k}_p \cdot \mathbf{r}) \hat{n}(\mathbf{r}) \\ &= \frac{1}{4}(\hat{n}_{\mathbf{k}_-} + \hat{n}_{-\mathbf{k}_-} + \hat{n}_{\mathbf{k}_+} + \hat{n}_{-\mathbf{k}_+}), \end{aligned} \tag{C5}$$

with $\hat{n}_q = \int d\mathbf{r} \hat{n}(\mathbf{r}) e^{i\mathbf{q}\mathbf{r}}$ being the Fourier transform of the fermionic density. Since $\tilde{\Delta}_c$ is the largest energy scale, ensuring that the coherent cavity dynamics are much faster than any other processes, the cavity photon field can be integrated out, which results in an effective long-range interaction Hamiltonian

$$H = H_{\mathrm{at}} + \int d\mathbf{r} d\mathbf{r}' D(\mathbf{r}, \mathbf{r}') \hat{n}(\mathbf{r}) \hat{n}(\mathbf{r}'), \tag{C6}$$

where the effective long-range interaction $D(\mathbf{r}, \mathbf{r}')$ is given in Eq. (1):

$$\begin{aligned}D(\mathbf{r},\mathbf{r}') = D_0[&\cos(\mathbf{k}_+ \cdot (\mathbf{r} - \mathbf{r}')) + \cos(\mathbf{k}_- \cdot (\mathbf{r} - \mathbf{r}')) \\ &+ \cos(\mathbf{k}_+ \cdot \mathbf{r} + \mathbf{k}_- \cdot \mathbf{r}') + \cos(\mathbf{k}_- \cdot \mathbf{r} + \mathbf{k}_+ \cdot \mathbf{r}')], \end{aligned} \tag{C7}$$

with the long-range interaction strength $D_0 = \eta_0^2/\tilde{\Delta}_c = U_0 V_0/\tilde{\Delta}_c$. We note that the two cavity modes couple to linearly independent combinations of DW operators $\hat{\Theta}_y$ and $\hat{\Theta}_z$; hence, within linearized equations of motion,

the two fields remain uncoupled. The main difference between the two terms is that the term $\hat{\Theta}_z$ couples to η_0 and the term $\hat{\Theta}_x$ couples to $\eta_0 \cos\phi$. In the following, we analyze the coupling of the fermionic atoms to only one cavity mode, as including the other is a straightforward extension.

APPENDIX D: INSTABILITY ANALYSIS AND EQUATIONS OF MOTION

1. General expression

In this appendix, we provide details on the general derivation of the growth rate equation [Eq. (2)]. For a single cavity mode, the Hamiltonian can be written as

$$H = H_{\mathrm{at}} + \frac{\tilde{\Delta}_c}{2}(\hat{x}^2 + \hat{p}^2) + \sqrt{2}\eta(t)x\hat{\Theta}, \tag{D1}$$

with x and p being the canonical quadrature operators $\hat{x} = (1/\sqrt{2})(\hat{a}^\dagger + \hat{a})$ and $\hat{p} = (i/\sqrt{2})(\hat{a}^\dagger - \hat{a})$. Here, $\hat{\Theta} = \hat{\Theta}_z$, and the long-range coupling strength $\eta(t) = \eta_0$ for $t > 0$ and $\eta(t) = 0$ before the quench. To compute the growth rate, we begin by using the linearized Heisenberg equations of motion, which, for the photon field, are

$$\dot{\hat{x}} = -\tilde{\Delta}_c \hat{p}, \qquad \dot{\hat{p}} = \tilde{\Delta}_c \hat{x} - \sqrt{2}\tilde{\Delta}_c \eta_0 \hat{\Theta}. \tag{D2}$$

Computing the equation of motion for the DW operator is complex, as its exact form depends on the microscopic details. However, we can utilize linear response theory to express the expectation value of the density operator:

$$n_{\mathrm{q}}(t) = \frac{\sqrt{2}}{4}\eta_0 N \int_{-\infty}^{\infty} dt' \chi(q, t-t')x(t'), \tag{D3}$$

where N is the total number of fermions in the cavity and $\chi(q,t)$ is the standard (intensive) density-density response function of the interacting fermions in the absence of the cavity [51]. Combining Eqs. (D2) and (D3), we obtain a second-order integro-differential equation for the expectation value of x:

$$\ddot{x} + \tilde{\Delta}_c^2 x - \frac{1}{8}\eta_0^2 N \tilde{\Delta}_c \int_{-\infty}^{\infty} dt' \sum_{q=\pm \mathrm{k}_\pm} \chi(q, t-t')x(t') = 0. \tag{D4}$$

As we are looking for quench instabilities, we consider an exponentially growing solution of the form $x(t) = x(0)e^{\alpha t}$ as an *ansatz*. This approach allows us to obtain a nonlinear, self-consistent equation for the instability growth rate α:

$$\alpha^2 + \tilde{\Delta}_c^2 - \frac{1}{8}\eta_0^2 N \tilde{\Delta}_c \sum_{q=\pm \mathrm{k}_\pm} \chi(q, \omega = i\alpha) = 0. \tag{D5}$$

Since the photon detuning is the largest energy scale, we neglect the α^2 term in the above equation, leaving D_0 as the only relevant experimental parameter. The final instability growth rate equation is

$$1 = \frac{1}{8}D_0 N \sum_{q=\pm \mathrm{k}_\pm} \chi(q, \omega = i\alpha). \tag{D6}$$

By neglecting the α^2 term, we simplify the dynamics, implying that the behavior of the cavity photons is not relevant to the instability. Instead, photons simply mediate the long-range interactions between fermions, with an amplitude determined by D_0. The above expression is equivalent to Eq. (2) by reexpressing $\chi(q, \omega = i\alpha)$ as an integral over real frequencies via the spectral representation [51].

2. RPA density response in the BEC-BCS crossover

In this section, we outline the derivation of the interacting fermion response function within the random-phase approximation (RPA), which captures the collective sound mode of the system, as well as the usual particle-hole continuum, which is gapped [52]. We follow the derivation of Refs. [40,53,54], where the approach is based on computing equations of motion of individual operators and then including the self-consistent field in a canonical way. The atomic Hamiltonian in momentum space reads

$$H_{\mathrm{at}} = \sum_k (\xi_k - \mu)\hat{c}_k^\dagger \hat{c}_k + U \sum_{k,k',q,\sigma,\sigma'} \hat{c}_{k+q,\sigma}^\dagger \hat{c}_{k'-q,\sigma'}^\dagger \hat{c}_{k',\sigma'} \hat{c}_{k,\sigma}, \tag{D7}$$

where ξ_k is the single fermion dispersion and U is an effective interaction strength, which satisfies the usual T-matrix scattering-length equation:

$$\frac{m}{4\pi a_s} = \frac{1}{U} + \frac{1}{V}\sum_{\mathrm{k}}^{k_c} \frac{m}{k^2}. \tag{D8}$$

We proceed by performing a mean-field decoupling and derive the BCS Hamiltonian:

$$H^0 = \sum_{k,\sigma} (\xi_k - \mu)\hat{c}_{k,\sigma}^\dagger \hat{c}_{k,\sigma} + \Delta \sum_k \hat{c}_{k,\uparrow}^\dagger \hat{c}_{k,\downarrow}^\dagger + \mathrm{H.c.} \tag{D9}$$

Using the Hamiltonian H^0, we can compute the individual response functions χ^0 due to external driving. To include the RPA response, we employ mean-field decoupling of the interacting Hamiltonian but also keep any term proportional to the expectation value of the operator we are driving, for example, $\langle \hat{n}_q \rangle$. Overall, this method gives rise to the RPA response function:

$$\chi^{\mathrm{RPA}} = \frac{\chi^0}{1 - U\chi^0(\sigma_x \oplus \sigma_x)}, \tag{D10}$$

where σ_x is a Pauli matrix. The above matrix equation should be understood as if acting on the vector $(\delta\hat{n}_{q\uparrow}, \delta\hat{n}_{q\downarrow}, \delta\hat{\Delta}, \delta\hat{\Delta}^\dagger)$, with $\hat{\Delta}_q^\dagger = \sum_k \hat{c}^\dagger_{k+q\uparrow}\hat{c}^\dagger_{-k\downarrow}$. By evaluating the entries and performing the matrix product, we obtain the expression for the density-density response of a homogeneous system. The above expression can now be generalized to the trap-averaged case by replacing it with [54]

$$\chi^{\mathrm{TA}}(q,\omega) = \int d\mathbf{r} n(\mathbf{r}) \chi^{\mathrm{RPA}}(q,\omega,n(\mathbf{r}),\Delta(\mathbf{r})), \quad \text{(D11)}$$

where $n(r)$ is the local density and $\Delta(r)$ is the local superfluid gap. Note that $n(\mathbf{r})$ satisfies $\int d\mathbf{r} n(\mathbf{r}) = N$, with N being the total atom number. We use this result in Eq. (2) to obtain the growth rate α.

APPENDIX E: NUMERICAL SIMULATIONS FOR SIMPLIFIED SYSTEMS

1. tMPS calculations in 1D

In this section, we show that the picture of the ordering dynamics has applicability beyond the three-dimensional Fermi gas described in the main text. In this regard, we study coupled cavity-atom systems, in which the atoms are confined to a one-dimensional lattice. In agreement with the experimental observations, we obtain an exponential ordering dynamics at early times, whose growth rate is mainly influenced by the strength of the long-range interactions.

In the following, we perform numerical simulations of one-dimensional interacting systems coupled to the field of the optical cavity. We recover the short-time dynamics of interest by employing a mean-field description of the cavity field. This approach neglects the fluctuations in the atom-cavity coupling [35,55,56]; however, it allows us to access larger sizes for the atomic system than in the simulations that treat the cavity field exactly [57,58]. Thus, we consider the following Hamiltonian for the coupled atom-cavity system [33,35]:

$$\begin{aligned} H &= H_{\mathrm{atoms}} + H_{\mathrm{ac}}, \\ H_{\mathrm{ac}} &= -\hbar\eta(\lambda_{\mathrm{c}}^* + \lambda_{\mathrm{c}}) \sum_j \cos(k_c j)\hat{n}_j, \end{aligned} \quad \text{(E1)}$$

where $\hat{n}_j$ is the atomic density operator and λ_{c} is a complex number describing the cavity field. The equation of motion of the cavity field is given by

$$\frac{\partial}{\partial t}\lambda_{\mathrm{c}} = i\eta \sum_j \cos(k_{\mathrm{c}} j)\langle \hat{n}_j \rangle - (i\tilde{\Delta}_{\mathrm{c}} + \kappa)\lambda_{\mathrm{c}}. \quad \text{(E2)}$$

For the results presented in this section, we consider the case in which the cavity is transversely pumped, with $\tilde{\Delta}_{\mathrm{c}}$ the detuning of the cavity with respect to the pump beam and the strength of the effective atom-cavity coupling given by η. The photon losses are controlled by the dissipation strength κ. As we are interested in the short-time dynamics, we do not include a stochastic Langevin noise term in Eq. (E2) [59], which would be relevant at later times. We choose the commensurability between the cavity wave vector and the one-dimensional lattice such that $k_c = \pi$; i.e., the cavity couples to the atomic odd-even density imbalance, $\sum_j (-1)^j \langle \hat{n}_j \rangle$.

To further emphasize the generality of our conclusions, for the atomic Hamiltonian, we consider interacting models for both spinful fermionic atoms:

$$\begin{aligned} H_{\mathrm{F}} &= H_{\mathrm{int}} + H_{\mathrm{kin}}, \\ H_{\mathrm{int}} &= U \sum_j \hat{n}_{j,\uparrow}\hat{n}_{j,\downarrow}, \\ H_{\mathrm{kin}} &= -J \sum_{j,\sigma} (\hat{c}^\dagger_{j,\sigma}\hat{c}_{j+1,\sigma} + \hat{c}^\dagger_{j+1,\sigma}\hat{c}_{j,\sigma}), \end{aligned} \quad \text{(E3)}$$

and bosonic atoms:

$$\begin{aligned} H_{\mathrm{B}} &= H_{\mathrm{int}} + H_{\mathrm{kin}}, \\ H_{\mathrm{int}} &= \frac{U}{2} \sum_{j=1}^{L} \hat{n}_j(\hat{n}_j - 1), \\ H_{\mathrm{kin}} &= -J \sum_{j=1}^{L-1} (\hat{b}^\dagger_j \hat{b}_{j+1} + \hat{b}^\dagger_{j+1}\hat{b}_j). \end{aligned} \quad \text{(E4)}$$

In both cases, J represents the tunneling amplitude and U the on-site repulsive interaction strength. In the presence of the cavity-induced global-range interactions, these models exhibit a phase transition to a density-wave-ordered state in their steady states as the atom-cavity coupling is increased [33,35].

While the cavity is treated at a mean-field level, we simulate the atomic dynamics numerically exactly. We employ a time-dependent matrix product state (tMPS) algorithm [60–62] for the Hamiltonian in Eq. (E1) while numerically integrating in parallel Eq. (E2). The initial state of the evolution corresponds to a state without any photons, $\lambda_{\mathrm{c}}(t=0) = 0$, and the atoms in the ground state of the model. The ground state is computed using the density matrix renormalization group (DMRG) algorithm in the matrix product state (MPS) representation [62,63]. The implementations make use of the ITensor Library [64].

We focus on the early times of the coupled atom-cavity dynamics, where we observe an exponential increase in the photon number, $n_{\mathrm{cav}} = |\lambda_{\mathrm{c}}|^2$. We obtain the exponential dynamics for all parameters considered and regardless of the statistics of the atomic model. We extract the growth rate of the exponential increase for different values of the atomic interactions and coupling η, presented in Fig. 5,

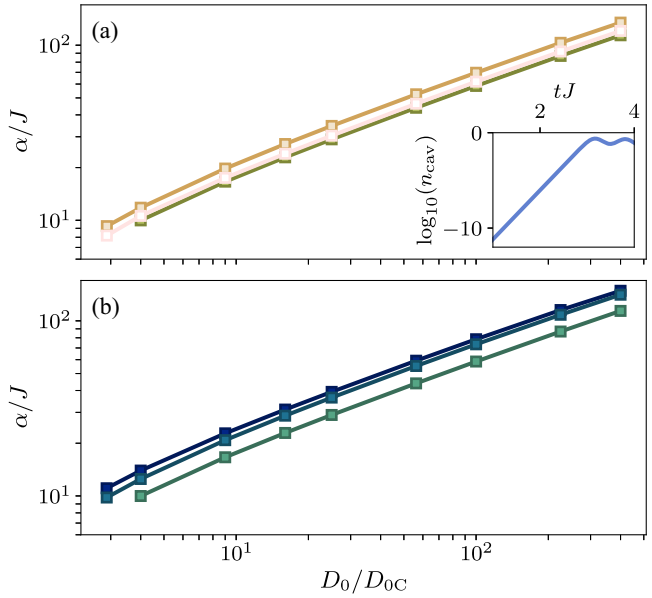

FIG. 5. One-dimensional cavity-atoms simulations. (a) Growth rate α in units of the hopping amplitude J as a function of $D_0/D_{0\mathrm{C}}$, obtained from the numerical simulations of Eqs. (E1) and (E2) for fermionic atoms, Eq. (E3), with on-site interaction strengths U/J: 0 (—), 4 (—), 16 (—). The inset shows the exponential growth of the intracavity photon number n_{cav} for a quench to $D_0/D_{0\mathrm{C}} = 4$ and $U/J = 4$ as a function of time t. (b) Growth rates for bosonic atoms, Eq. (E4), with U/J: 0.25 (—), 4 (—), ∞ (—). The parameters used for panels (a) and (b) are $\hbar\tilde{\Delta}_c/J = 200$ and $\hbar\kappa/J = 3.75$, considering a similar separation of scales as in the experiment. The simulations were performed for $L = 48$ sites and an atomic filling $N/L = 0.375$. The filling was chosen not to be commensurate with the potential induced by the cavity.

for parameters with similar scale separation as in the experiment. The critical value η_c has been determined by analyzing the self-organization phase transition, which occurs in the ground state of the Hamiltonian, Eq. (E1), computed self-consistently with the mean-field relations derived from the steady state of Eq. (E2). We observe that the main influence on the growth rate stems from the strength of the coupling to the cavity field η. Interestingly, we obtain very similar growth rates for both bosonic and fermionic atoms, for all values of the short-range interactions considered, ranging from noninteracting to strongly repulsive. This result further suggests that the exponential growth of the density wave order is mostly controlled by the strength of the long-range interactions while being only weakly influenced by the microscopic details of the atoms.

2. Gaussian state calculations in 2D

While linearized dynamics of the coupled atom-cavity system can be computed analytically and have good agreement with experiment, it is hard for it to predict how long the linear regime persists and thus how many decades of exponential growth there are. To estimate the duration of the exponential regime, we employ variational Gaussian states (GS) [65]. The variational parameters are the fermionic correlation matrix $\Gamma = \langle\psi_{\mathrm{GS}}|\hat{C}\hat{C}^\dagger|\psi_{\mathrm{GS}}\rangle$ and the photonic displacements $\Delta_{\mathrm{R}} = \langle\psi_{\mathrm{GS}}|(\hat{x},\hat{p})^T|\psi_{\mathrm{GS}}\rangle$, where $|\psi_{\mathrm{GS}}\rangle$ is the Gaussian wave function. In this way, we have the best possible description of the system up to two-point correlators. We perform a 2D square lattice discretization of the Hamitonian [Eq. (D1)] with nearest-neighbor hopping with hopping amplitude J for the kinetic term. We work in two dimensions instead of three since we do not expect solutions to change qualitatively for Gaussian states. We find the ground state for a given $U < 0$ in the absence of light, which is a BCS or BEC state, depending on the magnitude of U. We then apply a small noise transformation that preserves particle number to Γ and Δ_R, and we perform real-time evolution with the light-matter coupling quenched above the critical value. The equations of motion are

$$\begin{aligned} d_t\Delta_{\mathrm{R}} &= \sigma h_\Delta, \\ d_t\Gamma_{\mathrm{f}} &= i[\Gamma_{\mathrm{f}}, h_{\mathrm{f}}], \end{aligned} \tag{E5}$$

where $\sigma = \left(\begin{smallmatrix} 0 & -1 \\ 1 & 0 \end{smallmatrix}\right)$ and

$$\begin{aligned} h_\Delta &= 2\frac{\partial E}{\partial \Delta_{\mathrm{R}}}, \\ h_f &= -2\frac{\partial E}{\partial \Gamma_{\mathrm{f}}^{\mathrm{T}}}, \end{aligned} \tag{E6}$$

which are the derivatives of the expectation value of energy $E = \langle\psi_{\mathrm{GS}}|H|\psi_{\mathrm{GS}}\rangle$ in the time-dependent Gaussian state. Energy and particle number are conserved in the simulations. For simplicity, we take a single ordering wave vector $\mathbf{q} = (4\pi/L_x, 0)^T$. We expect translational invariance

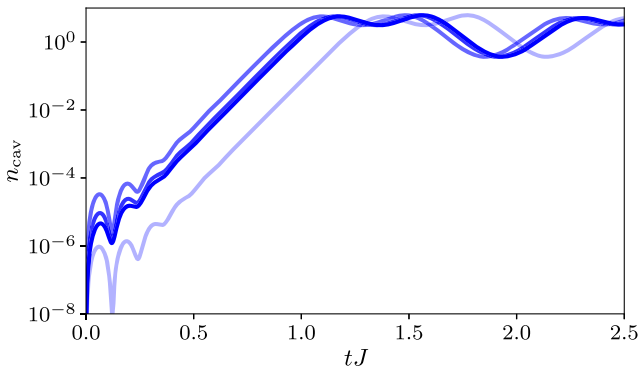

FIG. 6. Two-dimensional Gaussian state simulation. Intracavity photon number n_{cav} vs time t in units of the hopping amplitude J, following a deep quench into the DW-ordered phase for four repetitions of the quench simulation with random initial noise. The dynamics are modeled with variational Gaussian states and a lattice-discretized model.

in the perpendicular direction. The results shown here are for a lattice of $L_x \times L_y = 16 \times 4$ sites, but the computation has favorable scaling for much larger studies in the future. We set the filling factor to $\nu = 0.6$ so that the ratio $q/k_F \approx 0.4$ is close to the experimental value of k_-. We choose detuning $\tilde{\Delta}_c = 50J$ to have a good separation of scales. Figure 6 shows intracavity photon number versus time for a deep quench from a BEC state to $D_0/D_{0C} \gg 1$, with $U = -2J$, for four simulations. The dissipation is set to $\kappa = 2J$. We observe several decades of uninterrupted exponential growth, which qualitatively agrees with experiment. We also check that reducing or increasing dissipation does not significantly alter the duration of the linear regime.

[1] D. Baumann, *TASI lectures on inflation*, arXiv:0907.5424 (2012).

[2] A. Cavalleri, *Photo-induced superconductivity*, Contemp. Phys. **59**, 31 (2018).

[3] A. de la Torre, D. M. Kennes, M. Claassen, S. Gerber, J. W. McIver, and M. A. Sentef, *Colloquium: Nonthermal pathways to ultrafast control in quantum materials*, Rev. Mod. Phys. **93**, 041002 (2021).

[4] T. Albash and D. A. Lidar, *Adiabatic quantum computation*, Rev. Mod. Phys. **90**, 015002 (2018).

[5] L. E. Sadler, J. M. Higbie, S. R. Leslie, M. Vengalattore, and D. M. Stamper-Kurn, *Spontaneous symmetry breaking in a quenched ferromagnetic spinor Bose–Einstein condensate*, Nature (London) **443**, 312 (2006).

[6] C. N. Weiler, T. W. Neely, D. R. Scherer, A. S. Bradley, M. J. Davis, and B. P. Anderson, *Spontaneous vortices in the formation of Bose–Einstein condensates*, Nature (London) **455**, 948 (2008).

[7] L. Corman, L. Chomaz, T. Bienaimé, R. Desbuquois, C. Weitenberg, S. Nascimbène, J. Dalibard, and J. Beugnon, *Quench-induced supercurrents in an annular Bose gas*, Phys. Rev. Lett. **113**, 135302 (2014).

[8] N. Navon, A. L. Gaunt, R. P. Smith, and Z. Hadzibabic, *Critical dynamics of spontaneous symmetry breaking in a homogeneous Bose gas*, Science **347**, 167 (2015).

[9] L. Chomaz, L. Corman, T. Bienaimé, R. Desbuquois, C. Weitenberg, S. Nascimbène, J. Beugnon, and J. Dalibard, *Emergence of coherence via transverse condensation in a uniform quasi-two-dimensional Bose gas*, Nat. Commun. **6**, 6162 (2015).

[10] B. Ko, J. W. Park, and Y. Shin, *Kibble–Zurek universality in a strongly interacting Fermi superfluid*, Nat. Phys. **15**, 1227 (2019).

[11] S. Huh, K. Kim, K. Kwon, and J.-y. Choi, *Observation of a strongly ferromagnetic Spinor Bose-Einstein condensate*, Phys. Rev. Res. **2**, 033471 (2020).

[12] K. Lee, S. Kim, T. Kim, and Y. Shin, *Universal Kibble–Zurek scaling in an atomic Fermi superfluid*, Nat. Phys. **20**, 1570 (2024).

[13] A. B. Bardon, S. Beattie, C. Luciuk, W. Cairncross, D. Fine, N. S. Cheng, G. J. A. Edge, E. Taylor, S. Zhang, S. Trotzky, and J. H. Thywissen, *Transverse demagnetization dynamics of a unitary Fermi gas*, Science **344**, 722 (2014).

[14] R. J. Fletcher, R. Lopes, J. Man, N. Navon, R. P. Smith, M. W. Zwierlein, and Z. Hadzibabic, *Two- and three-body contacts in the unitary Bose gas*, Science **355**, 377 (2017).

[15] R. J. Fletcher, A. L. Gaunt, N. Navon, R. P. Smith, and Z. Hadzibabic, *Stability of a unitary Bose gas*, Phys. Rev. Lett. **111**, 125303 (2013).

[16] P. Makotyn, C. E. Klauss, D. L. Goldberger, E. A. Cornell, and D. S. Jin, *Universal dynamics of a degenerate unitary Bose gas*, Nat. Phys. **10**, 116 (2014).

[17] U. Eismann, L. Khaykovich, S. Laurent, I. Ferrier-Barbut, B. S. Rem, A. T. Grier, M. Delehaye, F. Chevy, C. Salomon, L.-C. Ha, and C. Chin, *Universal loss dynamics in a unitary Bose gas*, Phys. Rev. X **6**, 021025 (2016).

[18] C. Eigen, J. A. P. Glidden, R. Lopes, N. Navon, Z. Hadzibabic, and R. P. Smith, *Universal scaling laws in the dynamics of a homogeneous unitary Bose gas*, Phys. Rev. Lett. **119**, 250404 (2017).

[19] C. Sanner, E. J. Su, W. Huang, A. Keshet, J. Gillen, and W. Ketterle, *Correlations and pair formation in a repulsively interacting Fermi gas*, Phys. Rev. Lett. **108**, 240404 (2012).

[20] A. Amico, F. Scazza, G. Valtolina, P. E. S. Tavares, W. Ketterle, M. Inguscio, G. Roati, and M. Zaccanti, *Time-resolved observation of competing attractive and repulsive short-range correlations in strongly interacting Fermi gases*, Phys. Rev. Lett. **121**, 253602 (2018).

[21] J. Kanamori, *Electron correlation and ferromagnetism of transition metals*, Prog. Theor. Phys. **30**, 275 (1963).

[22] J. Dziarmaga, *Dynamics of a quantum phase transition and relaxation to a steady state*, Adv. Phys. **59**, 1063 (2010).

[23] L. De Marco, G. Valtolina, K. Matsuda, W. G. Tobias, J. P. Covey, and J. Ye, *A degenerate Fermi gas of polar molecules*, Science **363**, 853 (2019).

[24] X.-Y. Chen, A. Schindewolf, S. Eppelt, R. Bause, M. Duda, S. Biswas, T. Karman, T. Hilker, I. Bloch, and X.-Y. Luo, *Field-linked resonances of polar molecules*, Nature (London) **614**, 59 (2023).

[25] X. Zhang, Y. Chen, Z. Wu, J. Wang, J. Fan, S. Deng, and H. Wu, *Observation of a superradiant quantum phase transition in an intracavity degenerate Fermi gas*, Science **373**, 1359 (2021).

[26] V. Helson, T. Zwettler, F. Mivehvar, E. Colella, K. Roux, H. Konishi, H. Ritsch, and J.-P. Brantut, *Density-wave ordering in a unitary Fermi gas with photon-mediated interactions*, Nature (London) **618**, 716 (2023).

[27] M. Cetina, M. Jag, R. S. Lous, I. Fritsche, J. T. M. Walraven, R. Grimm, J. Levinsen, M. M. Parish, R. Schmidt, M. Knap, and E. Demler, *Ultrafast many-body interferometry of impurities coupled to a Fermi sea*, Science **354**, 96 (2016).

[28] G.-B. Jo, Y.-R. Lee, J.-H. Choi, C. A. Christensen, T. H. Kim, J. H. Thywissen, D. E. Pritchard, and W. Ketterle, *Itinerant ferromagnetism in a Fermi gas of ultracold atoms*, Science **325**, 1521 (2009).

[29] D. Pekker, M. Babadi, R. Sensarma, N. Zinner, L. Pollet, M. W. Zwierlein, and E. Demler, *Competition between pairing and ferromagnetic instabilities in ultracold Fermi gases near Feshbach resonances*, Phys. Rev. Lett. **106**, 050402 (2011).

[30] N. Defenu, T. Donner, T. Macrì, G. Pagano, S. Ruffo, and A. Trombettoni, *Long-range interacting quantum systems*, Rev. Mod. Phys. **95**, 035002 (2023).

[31] K. Baumann, C. Guerlin, F. Brennecke, and T. Esslinger, *Dicke quantum phase transition with a superfluid gas in an optical cavity*, Nature (London) **464**, 1301 (2010).
[32] J. Klinder, H. Keßler, M. Wolke, L. Mathey, and A. Hemmerich, *Dynamical phase transition in the open Dicke model*, Proc. Natl. Acad. Sci. U.S.A. **112**, 3290 (2015).
[33] H. Ritsch, P. Domokos, F. Brennecke, and T. Esslinger, *Cold atoms in cavity-generated dynamical optical potentials*, Rev. Mod. Phys. **85**, 553 (2013).
[34] V. D. Vaidya, Y. Guo, R. M. Kroeze, K. E. Ballantine, A. J. Kollár, J. Keeling, and B. L. Lev, *Tunable-range, photon-mediated atomic interactions in multimode cavity QED*, Phys. Rev. X **8**, 011002 (2018).
[35] F. Mivehvar, F. Piazza, T. Donner, and H. Ritsch, *Cavity QED with quantum gases: New paradigms in many-body physics*, Adv. Phys. **70**, 1 (2021).
[36] T. Bühler, T. Zwettler, G. Bolognini, A. Fabre, V. Helson, G. Del Pace, and J.-P. Brantut, *Direct production of fermionic superfluids in a cavity-enhanced optical dipole trap*, SciPost Phys. **18**, 133 (2025).
[37] Z. Wu, J. Fan, X. Zhang, J. Qi, and H. Wu, *Signatures of prethermalization in a quenched cavity-mediated long-range interacting Fermi gas*, Phys. Rev. Lett. **131**, 243401 (2023).
[38] S. Schütz, S. B. Jäger, and G. Morigi, *Dissipation-assisted prethermalization in long-range interacting atomic ensembles*, Phys. Rev. Lett. **117**, 083001 (2016).
[39] V. Subramanyan, S. S. Hegde, S. Vishveshwara, and B. Bradlyn, *Physics of the inverted harmonic oscillator: From the lowest Landau level to event horizons*, Ann. Phys. (N.Y.) **435**, 168470 (2021), special issue on Philip W. Anderson.
[40] L. He, *Dynamic density and spin responses of a superfluid Fermi gas in the BCS–BEC crossover: Path integral formulation and pair fluctuation theory*, Ann. Phys. (N.Y.) **373**, 470 (2016).
[41] K. Baumann, R. Mottl, F. Brennecke, and T. Esslinger, *Exploring symmetry breaking at the Dicke quantum phase transition*, Phys. Rev. Lett. **107**, 140402 (2011).
[42] A. Lamacraft, *Quantum quenches in a spinor condensate*, Phys. Rev. Lett. **98**, 160404 (2007).
[43] M. J. Bhaseen, J. Mayoh, B. D. Simons, and J. Keeling, *Dynamics of nonequilibrium Dicke models*, Phys. Rev. A **85**, 013817 (2012).
[44] O. L. Acevedo, L. Quiroga, F. J. Rodríguez, and N. F. Johnson, *New dynamical scaling universality for quantum networks across adiabatic quantum phase transitions*, Phys. Rev. Lett. **112**, 030403 (2014).
[45] N. Defenu, T. Enss, M. Kastner, and G. Morigi, *Dynamical critical scaling of long-range interacting quantum magnets*, Phys. Rev. Lett. **121**, 240403 (2018).
[46] T. Zwettler, G. Del Pace, F. Marijanovic, S. Chattopadhyay, T. Bühler, C.-M. Halati, L. Skolc, L. Tolle, V. Helson, G. Bolognini, A. Fabre, S. Uchino, T. Giamarchi, E. Demler, and J.-P. Brantut, 10.5281/zenodo.15371140 (2025).
[47] K. Roux, H. Konishi, V. Helson, and J.-P. Brantut, *Strongly correlated fermions strongly coupled to light*, Nat. Commun. **11**, 2974 (2020).
[48] K. Roux, V. Helson, H. Konishi, and J.-P. Brantut, *Cavity-assisted preparation and detection of a unitary Fermi gas*, New J. Phys. **23**, 043029 (2021).
[49] B. Gadway, D. Pertot, R. Reimann, M. G. Cohen, and D. Schneble, *Analysis of Kapitza-Dirac diffraction patterns beyond the Raman-Nath regime*, Opt. Express **17**, 19173 (2009).
[50] V. Helson, T. Zwettler, K. Roux, H. Konishi, S. Uchino, and J.-P. Brantut, *Optomechanical response of a strongly interacting Fermi gas*, Phys. Rev. Res. **4**, 033199 (2022).
[51] N. Dupuis, *Field Theory of Condensed Matter and Ultracold Gases* (World Scientific, Singapore, 2023), Vol. 1.
[52] R. Combescot, M. Y. Kagan, and S. Stringari, *Collective mode of homogeneous superfluid Fermi gases in the BEC-BCS crossover*, Phys. Rev. A **74**, 042717 (2006).
[53] H. Zhao, X. Gao, W. Liang, P. Zou, and F. Yuan, *Dynamical structure factors of a two-dimensional fermi superfluid within random phase approximation*, New J. Phys. **22**, 093012 (2020).
[54] A. Minguzzi, G. Ferrari, and Y. Castin, *Dynamic structure factor of a superfluid Fermi gas*, Eur. Phys. J. D **17**, 49 (2001).
[55] A. V. Bezvershenko, C.-M. Halati, A. Sheikhan, C. Kollath, and A. Rosch, *Dicke transition in open many-body systems determined by fluctuation effects*, Phys. Rev. Lett. **127**, 173606 (2021).
[56] S. B. Jäger, T. Schmit, G. Morigi, M. J. Holland, and R. Betzholz, *Lindblad master equations for quantum systems coupled to dissipative bosonic modes*, Phys. Rev. Lett. **129**, 063601 (2022).
[57] C.-M. Halati, A. Sheikhan, H. Ritsch, and C. Kollath, *Numerically exact treatment of many-body self-organization in a cavity*, Phys. Rev. Lett. **125**, 093604 (2020).
[58] C.-M. Halati, A. Sheikhan, and C. Kollath, *Theoretical methods to treat a single dissipative bosonic mode coupled globally to an interacting many-body system*, Phys. Rev. Res. **2**, 043255 (2020).
[59] C. Gardiner and P. Zoller, *Quantum Noise* (Springer-Verlag, Berlin, 2000).
[60] S. R. White and A. E. Feiguin, *Real-time evolution using the density matrix renormalization group*, Phys. Rev. Lett. **93**, 076401 (2004).
[61] A. J. Daley, C. Kollath, U. Schollwöck, and G. Vidal, *Time-dependent density-matrix renormalization-group using adaptive effective Hilbert spaces*, J. Stat. Mech. (2004) P04005.
[62] U. Schollwöck, *The density-matrix renormalization group in the age of matrix product states*, Ann. Phys. (N.Y.) **326**, 96 (2011).
[63] S. R. White, *Density matrix formulation for quantum renormalization groups*, Phys. Rev. Lett. **69**, 2863 (1992).
[64] M. Fishman, S. R. White, and E. M. Stoudenmire, *The ITensor Software Library for Tensor Network Calculations*, SciPost Phys. Codebases 4 (2022).
[65] T. Shi, E. Demler, and J. Ignacio Cirac, *Variational study of fermionic and bosonic systems with non-Gaussian states: Theory and applications*, Ann. Phys. (N.Y.) **390**, 245 (2018).